Article

First-Principles Study of Superabundant Vacancy Formation in Metal Hydrides

Changjun Zhang, and Ali Alavi

J. Am. Chem. Soc., **2005**, 127 (27), 9808-9817• DOI: 10.1021/ja050475w • Publication Date (Web): 16 June 2005

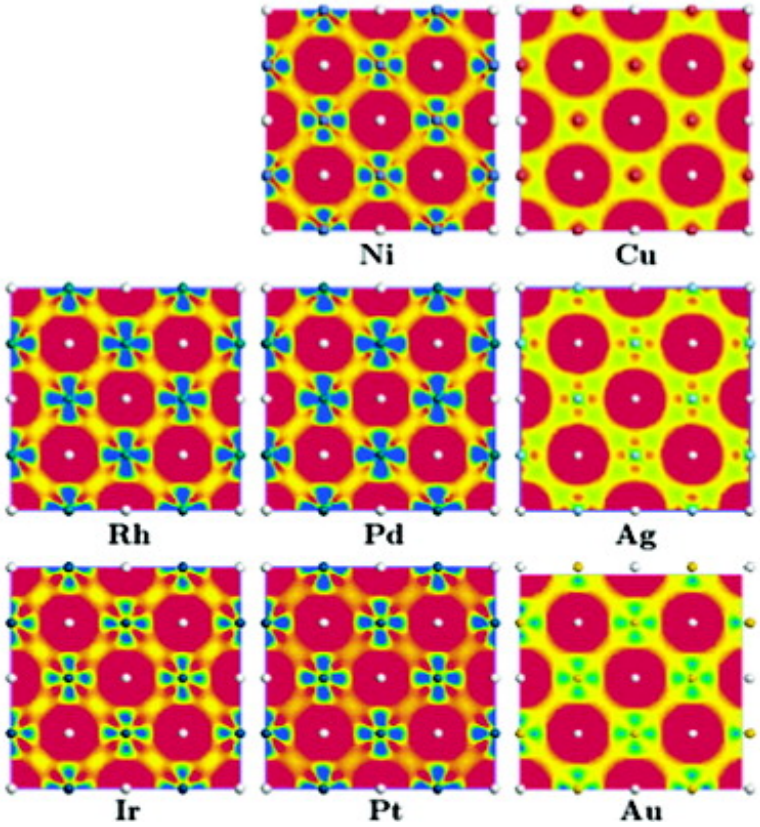

More About This Article

Additional resources and features associated with this article are available within the HTML version:

- Supporting Information
- Links to the 4 articles that cite this article, as of the time of this article download
- Access to high resolution figures
- Links to articles and content related to this article
- Copyright permission to reproduce figures and/or text from this article

J|A|C|S
ARTICLES
Published on Web 06/16/2005

First-Principles Study of Superabundant Vacancy Formation in Metal Hydrides

Changjun Zhang and Ali Alavi*

Contribution from the Department of Chemistry, University of Cambridge, Lensfield Road, Cambridge CB2 1EW, United Kingdom

Received January 24, 2005; E-mail: asa10@cam.ac.uk

Abstract: Recent experiments have established the generality of superabundant vacancies (SAV) formation in metal hydrides. Aiming to elucidate this intriguing phenomenon and to clarify previous interpretations, we employ density-functional theory to investigate atomic mechanisms of SAV formation in fcc hydrides of Ni, Cu, Rh, Pd, Ag, Ir, Pt, and Au. We have found that upon H insertion, vacancy formation energies reduce substantially. This is consistent with experimental suggestions. We demonstrate that the entropy effect, which has been proposed to explain SAV formation, is not the main cause. Instead, it is the drastic change of electronic structure induced by the H in the SAV hydrides, which is to a large extent responsible. Interesting trends in systems investigated are also found: ideal hydrides of 5*d* metals and noble metals are unstable compared to the corresponding pure metals, but the SAV hydrides are more stable than the corresponding ideal hydrides, whereas opposite results exist in the cases of Ni, Rh, and Pd. These trends of stabilities of the SAV hydrides are discussed in detail and a general understanding for SAV formation is provided. Finally, we propose an alternative reaction pathway to generate a SAV hydride from a metal alloy.

1. Introduction

Superabundant vacancies (SAV) are vacancies of metal atoms formed in metal hydrides, at concentrations as large as nearly 30 at. %. This novel discovery was reported first by Fukai et al. in 1994 in a X-ray diffraction study of the Pd−H system at high temperatures and high hydrogen pressures, where a vacancy-ordered phase of Cu_3Au structure (Pd_3VacH_4) was observed.[1] Since then, similar observations were made on many fcc hydrides of Ni, Rh, Pt, and Au and others,[2−7] and the H-induced SAV formation has now become a quite general phenomenon in metal hydrides. SAV formation has many important technological as well as scientific implications. For example, metal hydrides are regarded as a source of hydrogen for portable fuel cells,[8,9] and solubility of hydrogen can certainly be benefited from SAV formation; SAV structures are often found to be the most stable hydride structures and thus most of the phase diagrams of metal-H systems reported to date needs to be reinterpreted, and SAV formation may also provide clues for solving the long-standing problem of hydrogen embrittlement.[10] Therefore, understanding the physical reasons leading to SAV formation is of wide interest.

Despite receiving considerable attention, detailed mechanisms of SAV formation remain elusive. It had been known from early studies of plasmas-wall interaction in fusion reactors that implanted H isotopes can be trapped by implantation-induced vacancies.[11,12] This interesting finding has been investigated with effective-medium theory (EMT), and rather large binding energies of H to vacancies have been reported.[13,14] It was on the basis of this knowledge that Fukai et al. suggested the origin of SAV formation to be the lowering of the formation energy of a vacancy by trapping H atoms on its neighboring interstitial sites.[15] However, the accuracy and validity of the conclusions from EMT calculations have been questioned by recent First-principles density functional theory (DFT) studies on some H-vacancy complexes.[16] Another mechanism based on entropy effects has also been proposed to explain the SAV formation: an increase of the configurational entropy due to creation of metal vacancies should favor the SAV formation.[17] A recent calculation with cluster models evaluated the configurational entropy change to be ∼2.6 eV at ∼1000 K from Pd_4H_4 to Pd_3VacH_4,[18] and thus attributed the effect as the origin of the SAV formation. Considering that the vacancy formation energy in

(1) Fukai, Y.; Okuma, N. *Phys. Rev. Lett.* **1994**, *73*, 1640.
(2) Osono, H.; Kino, T.; Kurokawa, Y.; Fukai, Y. *J. Alloys Compd.* **1995**, *231*, 41.
(3) Watanabe, K.; Okuma, N.; Fukai, Y.; Sakamoto, Y.; Hayashi, Y. *Scripta Mater.* **1996**, *34*, 551.
(4) Hayashi, E.; Kurakawa, Y.; Fukai, Y. *Phys. Rev. Lett.* **1998**, *80*, 5588.
(5) Fukai, Y.; Shizuku, Y.; Kurokawa, Y. *J. Alloys Compd.* **2001**, *329*, 195.
(6) Fukai, Y.; Huchiarag, T.; Hayashi, E.; Ishii, Y.; Kurokawa, Y.; Yanagawa, J. *Defect Diffusion Forum* **2001**, *194*, 1063.
(7) Koike, H.; Shizuku, Y.; Yazaki, A.; Fukai, Y. *J. Phys.: Condens. Matter* **2004**, *16*, 1335.
(8) Schlapbach, L.; Züttel, A. *Nature* **2001**, *414*, 353.
(9) Grochala, W.; Edwards, P. P. *Chem. Rev.* **2004**, *104*, 1283.
(10) Fukai, Y. *J. Alloy. Comput.* **2003**, *73*, 1640.
(11) Möller, W.; Besenbacher, F.; Bøttiger, J. *Appl. Phys. A* **1982**, *27*, 19.
(12) Myers, S. M.; Richards, P. M.; Wampler, W. R.; Besenbacher, F. *J. Nucl. Mater.* **1989**, *165*, 9.
(13) Nordlander, P.; Nørskov, J. K.; Besenbacher, F. *J. Phys. F: Met. Phy.* **1986**, *16*, 1161.
(14) Nordlander, P.; Nørskov, J. K.; Besenbacher F.; Myers, S. M. *Phys. Rev. B* **1989**, *40*, 1990.
(15) Fukai, Y. *J. Alloys Compd.* **1995**, *231*, 35.
(16) Tateyama Y.; Ohno, T. *Phys. Rev. B* **2003**, *67*, 174105.
(17) Oates, W. A.; Wenzl, H. *Scripta Metall. Mater.* **1994**, *30*, 851; **1995**, *33*, 185.
(18) Watari, N.; Ohnishi, S. *J. Phys.: Condens. Matter* **2002**, *14*, 769.

10.1021/ja050475w CCC: $30.25

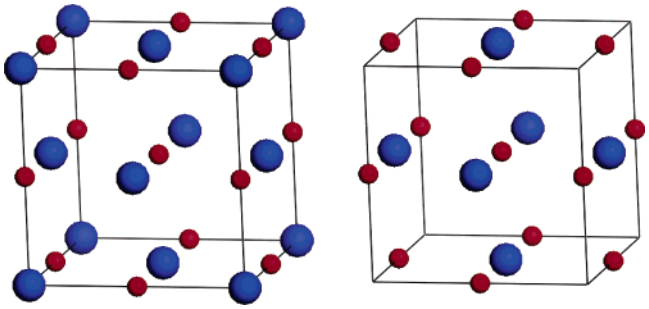

Figure 1. Unit cells of ideal hydride structure and SAV hydride structure. Metal atoms (at the face centers) are large blue, and hydrogen atoms are small red. In both cases, the most stable sites for hydrogen are the octahedral sites.

pure Pd is ~1.6 eV,[19] the reported entropy effect seems to be surprisingly large. In fact, by repeating the calculations used to evaluate the entropy change, we find that the actual value is about 10 times smaller than that reported. Therefore, their conclusion may be inappropriate.

In the present study, we employ first-principles DFT techniques using the supercell method with periodic boundary conditions. The reliability of such approaches to describe metal hydride systems has been verified in recent studies.[20−23] Our central objective is to clarify the SAV formation mechanisms, and to elucidate the generality of this intriguing phenomenon. To this end, we study a number of hydrides of fcc metals including Ni, Cu, Rh, Pd, Ag, Ir, Pt, and Au. Since the vacancy-ordered phase was reported experimentally to be the Cu_3Au type,[1] we chose all the SAV structures to be the same type. The structures of ideal and SAV hydrides are schematically shown in Figure 1. We have also examined the validity of this model in a larger unit cell (i.e., 32-metal atom cell), which will be discussed later. To illustrate the stability of the SAV structures, we compare in detail the energetics between the SAV hydrides and the ideal hydrides and the pure metals. Several effects, including zero-point energies, entropy effects and chemical potential of hydrogen are also taken into account. Aiming to shed light on the origin and the trend of SAV formation in the systems studied, detailed electronic structures of pure metals (M_4), defective metals (M_3Vac), ideal hydrides (M_4H_4), and SAV hydrides (M_3VacH_4) are presented and analyzed. As a side product, we also propose an alternative pathway to generate SAV in hydrides by alloying metals with the understanding accumulated from First-principles studies. The rest of the paper is organized as follows. In section 2, calculation details are outlined. Following this, the validity of our models is discussed by examining the configurations and energetics in large unit cells. In subsection 3.1, the calculated vacancy formation energies, cohesive energies, heats of formation of hydrides, etc are presented, and effects from zero-point energy, entropy and hydrogen chemical potential are discussed in subsection 3.2. In subsection 3.3, we carry out detailed electronic structure analyses. An attempt to generate a SAV hydride from an alloy is considered in subsection 3.4. Finally, our conclusions are summarized in the last section.

Table 1. Equilibrium Lattice Constants *a* (Å) and Bulk Moduli B_0 (GPa)

	lattice constant *a*		calcd. lattice constant *a*			bulk modulus B_0	
	calcd. (M_4)	expt.[a]	M_3Vac	M_4H_4	M_3VacH_4	calcd.	expt.[b]
Ni	3.53	3.52	3.40	3.74	3.61	202	186
Cu	3.60	3.61	3.46	3.87	3.72	147	137
Rh	3.84	3.80	3.80	4.04	3.89	271	270
Pd	3.90	3.89	3.75	4.08	3.93	209	181
Ag	4.11	4.09	3.96	4.35	4.16	108	101
Ir	3.85	3.84	3.71	4.06	3.90	341	355
Pt	3.96	3.92	3.80	4.17	4.00	269	278
Au	4.15	4.08	3.98	4.41	4.22	147	173

[a] See ref 27. [b] See ref 28.

2. Calculation Details

All calculations were performed using the plane-wave pseudopotential implementation of density-functional theory.[24] Exchange and correlation were treated within the Perdew−Burke−Ernzerhof (PBE) generalized gradient approximation (GGA).[25] The ionic cores were described by ultrasoft pseudopotentials,[26] which improve transferability and reduce the number of plane waves required in the expansion of the Kohn−Sham orbitals. The cutoff energy for the plane-wave expansion was set to be 400 eV, sufficiently high to give well-converged total energies and structures. The maximum k-point spacing used was no greater than 0.02 $Å^{-1}$, corresponding to a 12 × 12 × 12 (or 8 × 8 × 8) k-point mesh for a cubic supercell containing four (or 32) metal atoms. All structures including both cell parameters and the ionic positions were fully optimized so as to obtain the minimum total energies. The effect of spin polarization was also included throughout. With this setup, total energies in our calculations are converged to within ~0.01 eV. Our calculations reproduce accurately lattice constants[27] and bulk moduli[28] for all the metal systems studied, as shown in Table 1. The calculated lattice constants of metal hydride also compare well with experiments available, for example, in the cases of Ni and Pd hydrides, the calculated ones are 3.74 and 4.08 Å, very close to the experimental ones 3.72 Å[29] and 4.09 Å,[30] respectively. Also as expected, the insertion of H in metal leads to lattice expansion; and creation of metal vacancies leads to lattice contraction.

3. Results and Discussion

Before presenting our calculation results, it is worth discussing the supercell model chosen in this work. Our choice of the Cu_3-Au-type structure was motivated by the experimental findings of such a vacancy-ordered phase.[1,5] However, in such structures, the H atoms are constrained by symmetry and will remain in the ideal octahedral sites upon relaxation. Therefore, it would be interesting to examine the effects of atomic relaxation around vacancies and also the possibilities of existence of other SAV structures. For these purposes, we have tested structures of the ideal hydride and a number of ordered SAV hydrides in a larger unit cell of Pd (i.e., 32 metal atoms in the ideal cases). More disordered configurations are likely to be energetically unfavorable and thus not considered. The ideal hydride is schematically shown in Figure 2a. For the generation of the SAV structures, we considered first all the possible configurations of two metal vacancies in a 2 × 1 × 1 supercell (i.e., vacancies are nearest-

(19) Schaefer, H. E. *Phys. Status Solidi. A* **1987**, *102*, 47.
(20) Miwa K.; Fukumoto, A. *Phys. Rev. B* **2002**, *65*, 155114.
(21) Smithson, H.; Marianetti, C. A.; Morgan, D.; Van der Ven, A.; Predith, A.; Ceder, G. *Phys. Rev. B* **2002**, *66*, 144107.
(22) Caputo, R.; Alavi, A. *Mol. Phys.* **2003**, *101*, 1781.
(23) Wolverton, C.; Ozoliņš, V.; Asta, M. *Phys. Rev. B* **2004**, *69*, 144109.
(24) Payne, M. C.; Teter, M. P.; Allan, D. C.; Arias, T. A.; Joannopoulos, J. D. *Rev. Mod. Phys.* **1992**, *64*, 1045.
(25) Perdew, J. P.; Burke, K.; Ernzerhof, M. *Phys. Rev. Lett.* **1996**, *77*, 3865.
(26) Vanderbilt, D. *Phys. Rev. B* **1990**, *41*, 7892.
(27) Kittel, C. *Introduction to Solid State Physics*; Wiley: New York, 1971.
(28) Donohue, J. *The Structure of the Elements*; Wiley: New York, 1974.
(29) Mueller, W. M.; Blackledge, J. P.; Libowitz, G. G. *Metal Hydrides*; Academic Press: New York, 1968.
(30) Ross, D. K.; Antonov, V. E.; Bokhenkov, E. L.; Kolesnikov, A. I.; Ponyatovsky, E. G.; Tomkinson, J. *Phys. Rev. B* **1998**, *58*, 2591.

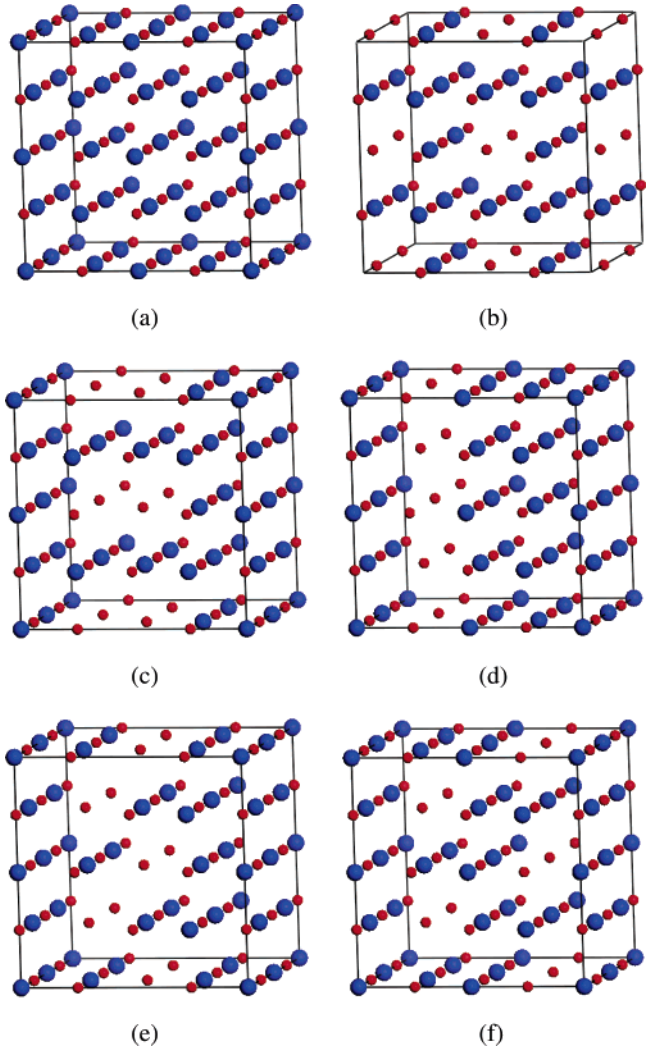

Figure 2. Structures in a (2 × 2 × 2) unit cell: (a) the ideal hydride; (b) the Cu_3Au-type SAV hydride; and (c−f) other less ordered SAV hydrides. Metal atoms are large blue, and hydrogen atoms are small red.

neighboring, next-nearest-neighboring and second-nearest-neighboring). We then duplicated these configurations in the 2 × 2 × 2 supercell, and obtained the ordered SAV hydrides (Figure 2b−f). Note that the structure in Figure 2b is essentially the Cu_3Au-type, and the others are less ordered. In the cases which correspond to the ideal hydride and the ordered Cu_3Au-type SAV hydride (Figure 2a,b), we have not found the H atoms to relax away from the ideal octahedral sites, although in the large cell the symmetry constraint was lifted and atomic relaxation could take place. Moreover, the energies per Pd calculated in the large unit cell are almost identical to those in the 4-Pd cell. In the cases which correspond to less ordered vacancy structures (Figure 2c−f), we have found significant relaxation of the H atoms away from the ideal octahedral sites. However, the energies of the less ordered vacancy structures are 0.15−0.17 eV (per Pd) higher than that of the more ordered one (Figure 2b), implying very large vacancy formation energies to form those structures. Therefore, the Cu_3Au-type structure is indeed the most favorable SAV structure, in agreement with the experiments.

3.1. Vacancy Formation Energy, Cohesive Energy and Heat of Formation. To investigate the vacancy formation in hydrides, it is instructive to examine first the vacancy formation energy (denoted as E_v) in pure metals. E_v is defined as

$$E_v = E(M_3Vac) + E(M,bulk) - E(M_4) \quad (1)$$

where the terms on the right-hand side refer to the total energies of defective metal, a single metal atom in the bulk and perfect metal, respectively, where all systems have been lattice-relaxed. Since vacancy formation energy is often understood from the cohesive energy (denoted as E_c), we also calculate E_c, which is the energy required to break the atoms of metals into isolated atomic species

$$E_c = -{}^1/_4(E(M_4) - 4E(M,isolated)) \quad (2)$$

As listed in Table 2, given the varied experimental conditions for the measurements, our calculated results are found to be in good agreement with the experiments (in parentheses),[19,31,32] in particular, the trends of E_v and E_c in these metals are well reproduced.

Conventionally, one would expect that the stronger the metal−metal bond, the harder it could be to break the bond and to create vacancies, i.e., the larger the E_c, the larger the E_v. Thus a simple empirical correlation has been proposed to understand E_v in the fcc metals

$$E_v \approx {}^1/_3E_{c'} \quad (3)$$

where the cohesive energy $E_{c'}$ is relative to a nonspinpolarized atomic state.[33] The empirical understanding of E_v in terms of E_c appears to be true in our results of each series of 3*d*, 4*d*, and 5*d* metals, however, not in same groups. For example, E_c in some 5*d* metals (Pt or Au) is much larger than E_c in some 4*d* metals (Pd or Ag), but E_v in the former is significantly smaller than E_v in the latter. The reason for this is because that the

Table 2. Calculated Vacancy Formation Energies in Metals (E_v), Cohesive Energies (E_c), Relaxation Energies (ΔE), Heats of Formation of Ideal Hydride ($\Delta H_{f,ideal}$) and SAV Hydrides ($\Delta H_{f,SAV}$), Vacancy Formation Energies in Hydrides ($E_{v,hydride}$) at Zero Temperature and Pressure, and Excluding ZPE[a]

	E_v[b]	E_c[c]	ΔE[d]	$\Delta H_{f,ideal}$[e]	$E_{v,hydride}$	$\Delta H_{f,SAV}$
Ni	1.43	4.78	1.02	−0.13	0.21	−0.08
	(1.4−1.8)	(4.44)		(0.26)		
Cu	0.99	3.65	0.91	0.52	−0.56	0.38
	(1.28−1.42)	(3.50)		(0.53)		
Rh	1.88	4.15	0.51	−0.16	0.43	−0.06
	(1.71)	(5.75)		(0.10)		
Pd	1.21	3.83	0.20	−0.25	0.43	−0.15
	(1.85 ± 0.25)	(3.94)		(−0.12,−0.20)		
Ag	0.73	2.64	0.62	0.69	−0.38	0.60
	(1.11−1.31)	(2.96)		(0.61)		
Ir	2.40	6.32	2.00	0.77	−1.77	0.33
	(1.97,2.70)	(6.93)		(0.75)		
Pt	0.74	4.92	3.78	0.40	−1.32	0.07
	(1.35 ± 0.09)	(5.86)		(0.20,0.59)		
Au	0.45	3.03	1.85	1.17	−1.67	0.75
	(0.89 ± 0.04)	(3.78)		(0.26)		

[a] Experimental data are in parentheses. All units are in eV. The effect of including ZPE and finite T and p is reported in Table 3. [b] Experimental data in brackets are from refs 19 and 31. [c] Experimental data in brackets are from ref 32. [d] ΔE is the relaxation energy, defined as the difference between $E_{c'}$ and $3E_v$. [e] Experimental data in brackets are from ref 34.

(31) de Boer, F. R.; Mattens, W. C. M.; Miedema, A. R.; Niessen, A. K. *Cohesion in Metals*; North-Holland: Amsterdam, 1988.
(32) Kittel, C. *Introduction to Solid State Physics*, 7th ed.; Wiley: New York, 1995.
(33) Górecki, T. *Z. Metallkd.* **1974**, *65*, 426.

above relation misses an important term, i.e., relaxation of the metal lattice upon creation of vacancies. If the relaxation is significant, the energy loss due to vacancy formation in metals would be largely compensated, and thus the vacancy formation energy would be much smaller than what the simple relation predicts. To evaluate the relaxation energy (ΔE) of the metal lattice, we calculated the differences between $E_{c'}$ and $3E_v$ and summarize them in Table 2. As can be seen that (i) in each series of the 3*d*, 4*d*, and 5*d* metals, the relaxation energies have similar magnitudes, and thus the dominant factor for the difference of E_v among those metals is the difference of E_c; (ii) in each of the three metal groups, the 5*d* metal has the largest relaxation energy, and thus the relaxation in the *5d* metal contributes more to compensate the energy loss due to vacancy formation than in the 3*d* and the 4*d* metal. In particular, the relaxation energies of Pt and Au are closer to their E_c, leading to the smaller E_v than those in Pd and Ag, respectively. The trend of relaxation energies is in fact consistent with the geometrical trend: the contraction of volume of the 5*d* metal is larger than that of the 3*d* and 4*d* metal in each group (Table 1), when going from M_4 to M_3Vac.

We turn now to the metal hydrides. In the most stable structures of ideal hydrides, the H was found to locate at the ideal octahedral sites (Figure 1a). We calculated the enthalpies of formation of the ideal hydrides ($\Delta H_{f,ideal}$) at zero pressure as follows

$$\Delta H_{f,ideal} = {}^1/_4(E(M_4H_4) - E(M_4) - 2E(H_2)) \qquad (4)$$

where all energies have been obtained from lattice-relaxed calculations. As listed in Table 2, Ni, Rh, and Pd hydrides have negative formation energies meaning that they are more stable than the corresponding pure metals, whereas all 5*d* metal hydrides and all group IB metal hydrides are unstable. Our calculated $\Delta H_{f,ideal}$ agree in general with the experimental data.[34] However they do not quite match Miedema's "law of reverse stability", which states that the more stable the metal (i.e., the larger the E_c), the less stable the hydride.[35] Again, like the relation of E_v and E_c as described above, the $\Delta H_{f,ideal}$ also cannot be understood solely from the E_c. We argue that the explanation neglects apparently the effect of the H insertion: upon H insertion, the newly formed H-metal bonding would certainly compensate the loss of cohesive energies of metals. We will discuss this later in terms of electronic structures.

In the SAV hydrides, the most stable occupation for H was again found to be on the interstitial octahedral sites. The SAV formation energy is defined as

$$E_{v,hydride} = E(M_3VacH_4) + E(M,bulk) - E(M_4H_4) \quad (5)$$

where the terms on the right refer to the total energies of the SAV hydride, single metal atom in the ideal bulk and ideal metal hydrides, respectively. The obtained results are also summarized in Table 2. Compared to pure metals, the vacancy formation energies are substantially reduced; in particular, in the cases of all 5*d* and group IB metals $E_{v,hydride}$ become negative. Since the vacancy formation energy reflects essentially the relative stabilities of ideal and SAV hydrides (i.e., a negative $E_{v,hydride}$ means that a SAV hydride is more stable than the corresponding ideal hydride), our calculated results reveal following interesting features. The SAV hydrides of Ni, Rh, and Pd are less stable than their ideal hydrides, whereas the SAV hydrides of all 5*d* metals and the noble metals are more stable than the ideal ones. Note that the $\Delta H_{f,ideal}$ of the ideal hydrides of Ni, Rh, and Pd are negative and those of the 5*d* and the noble metals are positive. Thus, it appears that if an ideal hydride is unstable compared to its corresponding pure metal, its SAV hydride would be more stable than the ideal hydride, and vice versa. It should be mentioned that similar results also occur in bcc metals, as our preliminary results suggest that the SAV hydrides of group VB metals (V,Nb,Ta) are less stable than the ideal hydrides, and the SAV hydrides of group VIB metals (Cr, Mo, W) are more stable than the ideal ones. Bear in mind that the heats of formation of the ideal hydrides in the former are significantly negative whereas those in the latter are significantly positive.[34]

We also consider the relative stabilities of SAV hydrides over pure metals by calculating heats of formation of the SAV hydrides, which are defined as

$$\Delta H_{f,SAV} = {}^1/_4(E(M_3VacH_4) + E(M,bulk) - E(M_4) - 2E(H_2)) \quad (6)$$

It can be seen from Table 2 that the $\Delta H_{f,SAV}$ has similar trends as $\Delta H_{f,ideal}$: SAV hydrides of Ni, Rh, and Pd are also more stable than pure Ni, Rh, and Pd metals, respectively. Interestingly, the magnitudes of $\Delta H_{f,SAV}$ of SAV hydrides of Ni, Rh, and Pd are less negative than those of $\Delta H_{f,ideal}$, whereas the magnitudes of $\Delta H_{f,SAV}$ of other SAV hydrides are less positive than those of the ideal counterparts, in particular, the SAV hydride of Pt becomes almost as stable as pure Pt metal. However, although SAV hydrides of Cu, Ag, Au, and Ir are more stable than their ideal counterparts, they are unstable compared to pure metals.

3.2. Zero-Point Energy, Entropy Effects and H_2 Chemical Potentials. In this section, we discuss several factors affecting the stabilities of SAV hydrides, including zero-point energy (ZPE), entropy and H_2 chemical potentials.

The high temperature (T) and pressure (p) applied in experiments can affect significantly the H_2 chemical potential, and consequently the stabilities of hydrides with respect to the pure systems. Therefore, we first discuss the effect of the H_2 chemical potential. In doing so, we replace the total energy of H_2 ($E(H_2)$) in eqs 4 and 6 as the H_2 chemical potential ($\mu_{H_2}(T,p)$), which is defined as

$$\mu_{H_2}(T,p) = E(H_2) + \mu_{H_2}(T,p^0) + k_bT\ln(p_{H_2}/p^0) \qquad (7)$$

where p^0 is the atmospheric pressure and $\mu_{H_2}(T,p^0)$includes the contribution from rotations and vibrations of the molecule as well as the ideal-gas entropy at 1 atm (here we use experimental values from thermodynamic tables). We took T and p as 1000 K and 5 GPa respectively, (which roughly correspond to the experimental conditions), and calculated the heats of formation of ideal and SAV hydrides by using the above equation. As shown in Table 3, both the ideal and the SAV hydrides are destabilized by ~0.29 eV compared to the zero T and p results. This is because, although the high pressure raises the chemical potential of H_2, the high temperature lowers it considerably (via

(34) Griessen, R.; Driessen, A. *Phys. Rev. B* **1984**, *30*, 4372.
(35) Miedema, A. R. *J. Less-Common Met.* **1973**, *32*, 117.

Table 3. Compared to the Zero T and p Results, the Effects of the H_2 Chemical Potential (μ_{H2}), the Zero-Point Energy ($\Delta(ZPE)$), the Configurational and Vibrational Entropies ($-T\Delta S$) on $\Delta H_{f,ideal}$, $E_{v,hydride}$ and $\Delta H_{f,SAV}$[a]

	$\Delta H_{f,ideal}$				$E_{v,hydride}$				$\Delta H_{f,SAV}$			
	μ_{H_2}	$\Delta(ZPE)$	$-T\Delta S$	overall	μ_{H_2}	$\Delta(ZPE)$	$-T\Delta S$	overall	μ_{H_2}	$\Delta(ZPE)$	$-T\Delta S$	overall
Ni	0.29	−0.05	0.00	0.11	0.00	0.11	−0.24	0.08	0.29	−0.02	−0.06	0.12
Cu	0.29	−0.04	0.00	0.77	0.00	0.08	−0.27	−0.74	0.29	−0.02	−0.06	0.58
Rh	0.29	−0.07	0.00	0.05	0.00	0.14	−0.30	0.27	0.29	−0.03	−0.07	0.12
Pd	0.29	−0.10	0.02	−0.05	0.00	0.17	−0.38	0.23	0.29	−0.06	−0.08	0.00
Ag	0.29	−0.04	0.00	0.94	0.00	0.04	−0.24	−0.59	0.29	−0.04	−0.05	0.79
Ir	0.29	−0.11	0.01	0.95	0.00	0.28	−0.25	−1.73	0.29	−0.04	−0.05	0.53
Pt	0.29	−0.12	−0.01	0.57	0.00	0.15	−0.24	−1.41	0.29	−0.08	−0.07	0.21
Au	0.29	−0.13	0.05	1.38	0.00	0.25	−0.33	−1.75	0.29	−0.06	−0.04	0.95

[a] Taking into account all the above effects, the overall results are also summarized. All units are in eV.

the $\mu_{H2}(T,p^0)$term) and consequently the overall effect does not favor hydride formation (either the ideal or the SAV hydride). Note that the chemical potential of H_2 is significantly temperature dependent: a use of a lower temperature of 700 K would only destabilize the hydrides by ~0.15 eV, in which case the stabilities of hydrides of some metals (say, Pd) would be significantly different from those at 1000 K. Note too that the vacancy formation energies remain the same as the zero T and p results, because the H_2 chemical potential at high T and p exerts same effects on the ideal and SAV hydrides. In other words, the stability of the SAV hydride relative to the ideal hydride is unaffected by the chemical potential of H_2.

ZPE is also significant in hydrides due to the light mass of the H atoms. In some cases, ZPE is the dominant factor for determining the most stable interstitial site.[22] Here we calculated ZPE for all the hydride systems within the harmonic approximation. The harmonic modes of H motions were calculated from a finite difference approach. Briefly, the dynamical matrix $D_{i\alpha,j\beta}$ is obtained by displacing each Cartesian component $x_{i\alpha}$ of each atom i by a finite amount $\pm\delta x_{i\alpha}$, and computing the resulting forces by performing a self-consistent minimization of the total energy functional

$$D_{i\alpha,j\beta} = \frac{1}{(m_i m_j)^{1/2}} \frac{F_j\beta(\delta_{xi\alpha}) - F_{j\beta}(-\delta x_{i\alpha})}{2\delta x_{i\alpha}} \qquad (8)$$

where m_i is the mass of atom i. Including the ZPE obtained for the ideal hydrides, the SAV hydrides, and the H_2, we list the ZPE in the calculation of the heats of formation of ideal and SAV hydrides, and vacancy formation energies in Table 3. As can be seen the ZPE reveals different effects on the ideal and SAV hydrides: ZPE is generally larger in the SAV hydrides than in the ideal hydrides. As a result, the vacancy formation energies including ZPE is more positive than that excluding ZPE. In other words, the ZPE favors the formation of the ideal hydrides.

We approximate the entropy effects as arising mainly from configurational and vibrational contributions. The configurational entropy should favor the SAV formation. This is because that due to formation of metal vacancies, the number of ways to arrange metal atoms to obtain degenerate configurations in SAV hydrides increases, compared to that in ideal hydrides. To evaluate the configurational entropy change from ideal hydrides to SAV structures (denoted as ΔS_{config}), we first consider the number of ways to arrange n metal atoms in m possible lattice sites, i.e., C_n^m, then suppose the vacancy concentration $C_v = (m - n/m)$, and deduce the (ideal, upper-bound) configurational entropy per site as

$$\Delta S_{config} = -k_b[C_v \ln C_v + (1 - C_v)\ln(1 - C_v)] \qquad (9)$$

At 1000 K the total configurational entropy change is calculated to be 0.19 eV. Note that this value is the same in all the present cases. It should be mentioned that the entropy evaluated here is based on the Cu_3Au-type hydrides. In larger unit cell there exists other possible SAV configurations, which need to be taken into account. However, as we showed in the beginning of the discussion, the total energies of those configurations are far too large compared to the Cu_3Au-type one and thus it is justified to neglect their contribution to the configurational entropy.

In a previous study, the vibrational entropy of the lattice was approximated as just the Boltzmann constant.[18] Considering the complexity of the systems, this approximation is too simple. In general, the dominant contribution to the vibrational entropy (S_{vib}) comes from low-energy modes, and these are from the acoustic branches of the phonon dispersion curves. Since these are very difficult to calculate from our first-principles approach, we resort to an approximation, namely the Debye model.[36] In three-dimensions ($d = 3$) the Debye vibrational entropy is

$$S_{vib}(T)/Nk_b = d\int_{(\Theta_D/T)}^{\infty} \frac{dx}{e^x - 1} + d(d+1)(T/\Theta_D)^d \int_0^{(\Theta_D/T)} \frac{x^d\,dx}{e^x - 1} \qquad (10)$$

where Θ_D is the Debye temperature, which physically represents the highest frequency in the acoustic mode spectrum, and mathematically provides the cutoff for integrals over the modes. The Debye temperature is evaluated as

$$\Theta_D = \left(\frac{3}{4\pi}\right)^{1/6} \frac{h}{k_b} \sqrt{\frac{r_{WS}B}{M}} \qquad (11)$$

where r_{WS} is the equilibrium Wigner-Seitz radius, M is the atomic weight, and B is the bulk modulus. This approach has been proved to be quite accurate in recent studies.[37] With this method, we found that the bulk moduli and subsequently the Debye temperatures in SAV hydrides are generally smaller than those in ideal hydrides, and thus ΔS_{vib} from ideal to SAV hydrides is positive. In other words, the vibrational contribution also favors the SAV formation. The magnitudes of the ΔS_{vib} obtained between ideal and SAV hydrides are within a range from 0.05 to 0.18 eV.

(36) Feibelman P. J.; Alavi, A. *J. Phys. Chem. B* **2004**, *108*, 14362.
(37) Moroni, E. G.; Grimvall, G.; Jarlborg, T. *Phys. Rev. Lett.* **1996**, *76*, 2758.

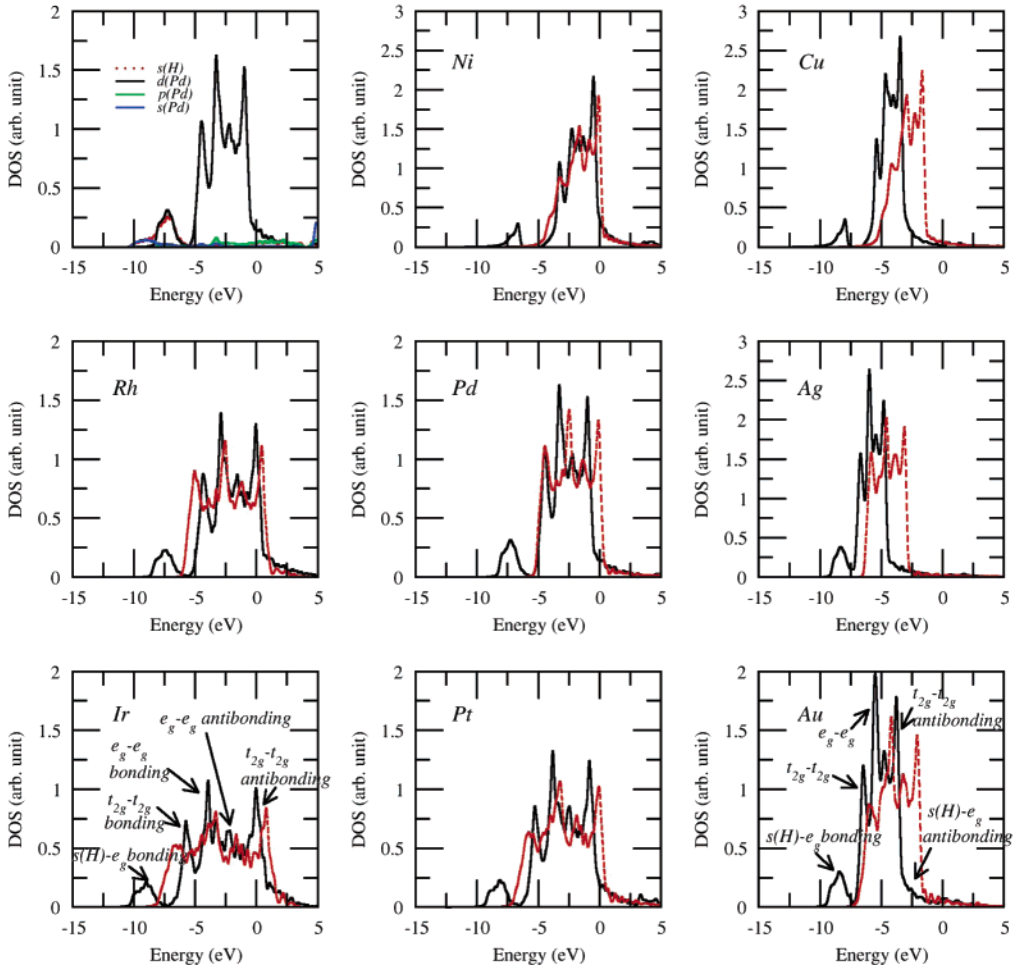

Figure 3. Top left panel: the density of states (DOS) projected onto the *s* orbital of H and the *d*, *p* and *s* orbitals of metal in the case of PdH. The rest: DOS projected onto metal *d* orbitals in ideal metals (dashed curves) and ideal hydrides (solid curves). Fermi levels are zeroed. In Ir and Au cases, characters of DOS peaks are indicated. Similar features occur in other cases.

Taking into account all the above effects, we summarize in Table 3 the overall results of $\Delta H_{\mathrm{f,ideal}}$, $E_{\mathrm{v,hydride}}$, and $\Delta H_{\mathrm{f,SAV}}$. We find that all these effects do not alter the main trend obtained at the zero *T* and *p* calculations, i.e., the substantial reduction of the vacancy formation energies from metals to hydrides. Moreover, the entropy effect, the only effect to facilitate the SAV formation, is small compared to the change of the vacancy formation energies. Therefore, the substantially reduced vacancy formation energies are the main factor in the understanding of the SAV formation, consistent with experimental suggestions. However, there are two points of note from Table 3. First, in the cases of Ni, Rh, and Pd, there exist some energy barriers (although may not significant, say, in the Ni case) for the SAV formation if the reaction were to occur via the ideal hydrides. Thus, we suggest an alternative pathway for the SAV hydride formation, i.e., via the hydrogenation of metals. Although Table 3 shows that the SAV hydrides of Ni, Rh, and Pd are unstable with respect to pure metals, their $\Delta H_{\mathrm{f,SAV}}$ would all become negative if a low temperature (say, 700 K) were used in the calculation of the H_2 chemical potential as we discussed earlier. Therefore, this SAV formation pathway may become feasible at low temperatures, although the kinetic rate constant of the SAV formation becomes small at low temperature. Second, in the cases of other metals, both ideal and SAV hydrides are clearly unstable with respect to their corresponding metals, and thus it becomes more difficult to form SAV although the SAV hydrides are more stable than the ideal hydrides. These results perhaps are consistent with the experimental fact that the findings of SAV formation in fcc metal hydrides were reported mainly in the Ni and Pd cases.

3.3. Electronic Structure Analysis. From above results and discussion, the central question in SAV formation mechanism is to understand why the vacancy formation energies reduce substantially from metals to hydrides. On the basis of eqs 1 and 5, the answer must be that the energy of $E(M_3VacH_4) - E(M_4H_4)$ is more negative than that of $E(M_3Vac) - E(M_4)$, or put it in another way, $E(M_3VacH_4) - E(M_3Vac) < E(M_4H_4) - E(M_4)$. This indicates that the defective metals (M_3Vac) must be stabilized by the H-metal bonding in M_3VacH_4 to somewhat greater extents than the ideal metals are stabilized, if at all, by the H-metal bonding in M_4H_4. In particular, the differences between $E(M_3VacH_4) - E(M_3Vac)$ and $E(M_4H_4) - E(M_4)$ should be greater in the cases of 5*d* and noble metals than those in other cases. To elucidate the origin of these results, we next examine the electronic structures of all the systems involved, i.e., M_4, M_3Vac, M_4H_4, and M_3VacH_4.

In Figure 3 we plot the density of states (DOS) projected onto metal atoms in pure metal systems and ideal hydrides. For the sake of clarity, we only show the DOS projected onto *d* orbitals of the metals since contributions of *d* orbitals are

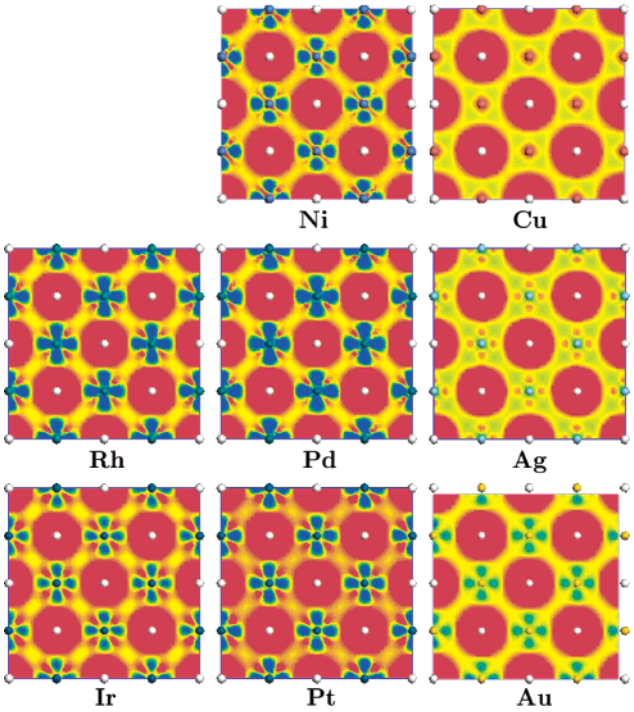

Figure 4. Electron density difference upon hydride formation. In all cases, the slices are cut through the (001) plane of the fcc structures and are shown with the same scale. Red or gray (in black/white) areas indicate electron accumulations and blue or dark (in black/white) areas indicate electron depletions. The hydrogen atoms are white and metal atoms are colored.

dominant in the total DOS. The 1*s*(H)-*s*(M), and 1*s*(H)-*p*(M) interactions are much smaller than the 1*s*(H)-*d*(M) interaction, as illustrated in the top left panel of Figure 3, where the PdH is chosen as an example. In the rest of the Figure, results are arranged in the same order as that of metal positions in the periodic table and in all cases the Fermi levels are zeroed. Let us first consider the DOS in M_4, which are shown as dashed curves. Our results reproduce the conventional picture of electronic structures of metals (i.e., the Friedel model).[38] As we move across each series of 3*d*, 4*d*, or 5*d* metals, the Fermi level moves up in the *d* band and metal is destabilized by the filling of states with antibonding characters. As results, the cohesive energy decreases. Note that the Fermi levels are in fact well above the *d*-band in the cases of group IB metals, because of fully filled *d*-bands in those metals. Additionally, the *d*-bands are narrow compared to group VIII metals. This is because the relatively large nuclear charge in group IB reduces the extent and overlap of the *d*-bands.

In the DOS of ideal hydrides (solid curves in Figure 3), new features can be seen by comparing with the DOS of pure metals. In the cases of group VIII metal hydrides, significant H-induced e_g-e_g bonding features appear at low energy levels, and the Fermi levels shift downward in hydrides compared to metals. These indicate the H-metal bond formation. Moreover, the second lowest peaks that featured mainly with $t_{2g}-t_{2g}$ bonding characters move toward high energy levels compared to metals, reflecting the weakening of the metal−metal bond upon H insertion. Interestingly, the upward movement becomes less significant when moving across the same *d* series, and more significant when moving down the same group. In other words,

(38) Friedel, J. *The Physics of Metals*; Ziman, J. M., Ed.; Cambridge University Press: Cambridge, 1969.

Table 4. Charges of Metals (e_M) and *d* Electron Gains from Metals to Hydrides (e_d) in the Cases of Ideal Hydrides and SAV Hydrides

	Rh	Ir	Ni	Pd	Pt	Cu	Ag	Au
Ideal Hydrides								
(i) e_M	+0.24	+0.11	+0.20	+0.12	+0.10	+0.22	+0.25	+0.09
(ii) e_d	−0.13	−0.23	−0.14	−0.12	−0.19	−0.01	0	+0.01
SAV hydrides								
(i) e_M	+0.35	+0.25	+0.30	+0.17	+0.20	+0.32	+0.34	+0.19
(ii) e_d	−0.06	−0.16	−0.11	−0.09	−0.15	+0.05	+0.05	+0.07

from right to left in the same *d* series or from the top to bottom in the same group, the metal−metal bond weakening costs more and more energy due to the H insertion. These results coincide well with the trend of formation enthalpies of ideal hydrides. For instance, in the same series, $\Delta H_{f,ideal}(Pd_4H_4)$ (or $\Delta H_{f,ideal}(Pt_4H_4)$) is more negative than $\Delta H_{f,ideal}(Rh_4H_4)$ (or $\Delta H_{f,ideal}(Ir_4H_4)$); in the same group, the 5*d* metal hydrides is the least unstable. In the cases of group IB metals hydrides, there exist somewhat different electronic features from above. First, there are no upward movements of the $t_{2g}-t_{2g}$ peaks. This is because that the noble metals have much smaller cohesive energies than others, and thus the relatively less significant weakening of $t_{2g}-t_{2g}$ bonding due to H insertion could be easily compensated by the H-metal bonding. Second, there are some H(*s*)-metal(e_g) antibonding states on top of the *d* bands, for example, between ~ -3 eV to the Fermi level in the case of Au_4H_4 (Figure 3). Clearly, these antibonding states are responsible for the large positive formation energies of hydrides of noble metals. Note that the similar states also exist in hydrides of group IIIV metals, but they are unoccupied and above the Fermi levels. It is worth mentioning that our results agree well with previously reported electronic structures. For example, in the PdH case, our DOS reproduce the main features reviewed by Gupta and Schlapbach:[39] the low-lying bonding states have *s*-e_g characters; these states are centered around 7.4 eV; and the metal *d*-bands are narrowed compared to pure Pd.

More insight can be obtained by examining charge transfer upon hydride formation. In Figure 4 we plot the total electron density difference by subtracting the total electron density in metals (with exactly same structures as those in hydrides but without H) from that in hydrides. Remarkably clear charge accumulations (the red or gray areas in black/white print) in H can be seen in each case, indicating the negatively charged H in hydrides. Moreover, in ease case of group IIIV metals and hydrides there are significant charge depletions on metals (the blue or dark areas in black/white print), which feature with some metal e_g states, and noticeable charge accumulations on metal t_{2g} states (the red or gray areas in black/white print). This shows that H not only attracts electrons from metals, but also induces electron redistribution within metals themselves. On one hand, the e_g electron loss on metals and the electron gain on H mean the strengthening of metal-H bonds and lowering the energies of systems. On the other hand, the *d* electron gain in metals means that the electrons must be promoted to the top of *d* bands, which feature coincidently with $t_{2g}-t_{2g}$ antibonding characters (Figure 3), and thus increase the energies of systems. It should be mentioned that a recent LDA study on hydrides of 3*d* metals also reveal similar features of *d* electron loss and gain,[21] although

(39) Gupta, M.; Schlapbach, L. *Topics in Appl. Phys.* **1988**, *63*, 139.

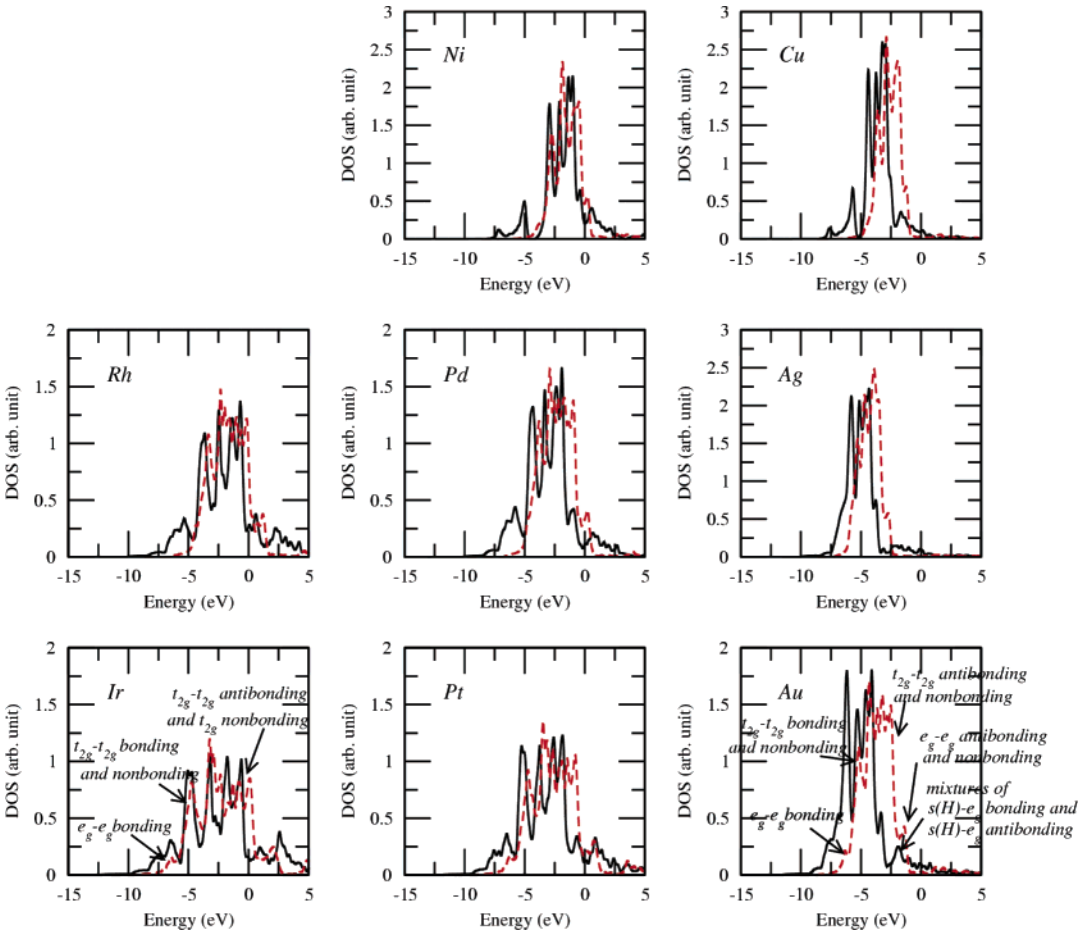

Figure 5. Density of states (DOS) projected onto metal *d* orbitals in M_3Vac (dashed curves) and SAV hydrides (solid curves). Fermi levels are zeroed. In, Ir, and Au cases, characters of DOS peaks are indicated. Similar features occur in other cases.

4*d* and 5*d* series were not considered. In the present study it is evident from Figure 4 that in Ni, Rh, and Pd cases, the electron losses in metals are large and the electron gains are small, whereas quite opposite results exist in Ir and Pt cases. To further support this, we list in Table 4 charges of metal atoms in hydrides and *d* electron gains (from M_4 to M_4H_4) on metal atoms from Mulliken charge analysis. The Mulliken analysis is performed using a projection of the plane-wave states onto a localized basis using the formalism described by Segall et al.[40] As can be seen, in Pt and Ir hydrides the metal charges are less positive and the *d* electron gains are more significant than those in Ni, Pd, and Rh hydrides. These indicate clearly that the hydrides of the 5*d* metals are less stable than other hydrides. In the cases of group IB metals and hydrides, the *d*-states are filled so that there are only negligible *d* electron losses and gains from M_4 to M_4H_4, as also can be seen from Figure 4. Therefore, the bonding between H and these metals is weak.

Next we discuss the DOS of M_3Vac and M_3VacH_4, which are shown in Figure 5. Compared to M_4, DOS of M_3Vac (dashed curves in Figure 5) reveal some new features due to the vacancy formation. Again, we discuss first the group VIII metals and hydrides. At the lowest energy a small peak emerges (for example, at ~6.5 eV in the Ir case) and it has e_g-e_g bonding characters. The second lowest peak (for example, at ~ −5.0 eV in the Ir case) has mainly some $t_{2g}-t_{2g}$ bonding characters and some t_{2g} nonbonding characters. Furthermore, due to vacancy formation the e_g-e_g and particularly the $t_{2g}-t_{2g}$ bonding states in M_3Vac are more localized and are significantly higher in energy than those in M_4. This is because that the $t_{2g}-t_{2g}$ bonding is along the metal−metal axis and thus the vacancy formation affects the $t_{2g}-t_{2g}$ states more than it does on the e_g-e_g states. Near the Fermi level, in addition to $t_{2g}-t_{2g}$ antibonding states, t_{2g} nonbonding characters can also be seen. These features have important implications when hydriding the M_3Vac. First, like ideal hydrides, upon H insertion to M_3Vac there are also H(*s*)-metal(*d*) bonding features and downward movements of the Fermi levels (solid curves in Figure 5). More importantly, more extensive $s-e_g$ bonding is formed in M_3VacH_4 than M_4H_4, evidenced by the more pronounced peaks. This is due to the more localized e_g states in M_3Vac than in M_4, making them more easily to form bonding with H. Second, unlike ideal hydrides, the second low-energy states featured mainly with $t_{2g}-t_{2g}$ bonding and nonbonding characters in SAV hydrides move downward compared to the corresponding metals. This is mainly because that the t_{2g} nonbonding states can form bonding with H(*s*) and thus decrease energies of the systems. We also carried out Mulliken charge analyses on M_3Vac and M_3VacH_4. As summarized in Table 4, in M_3VacH_4 the charge transfers from metals to H are generally more significant than those in M_4H_4, indicating the stronger H-metal interaction than in M_4H_4. On the other hand, the *d* electron gain in metals in M_3VacH_4 is less significant than in M_4H_4.

(40) Segall, M. D.; Pickard, C. J.; Shah, R.; Payne, M. C. *Mol. Phys.* **1996**, *89*, 571.

Moreover, because states at or just below the Fermi levels in M_3VacH_4 feature with some nonbonding states, the electrons added to the top of the occupied states do not increase the energy as much as in M_4H_4. All these indicate that H insertion indeed stabilizes M_3Vac more than it does on M_4. Therefore, this is the reason responsible for the reduction of vacancy formation energies in hydrides compared to those in metals. In addition, because 5*d* metals have more diffuse *d* states (i.e., lower e_g-e_g bonding states) than 3*d* and 4*d* metals, the metal-H bonding in 5*d* SAV hydrides should benefit more from the lower energy e_g(metal)$-s$(H) bonding states than in 3*d* and 4*d* ones. On the other hand, due to the much less *d* electron gain in SAV hydrides than in ideal hydrides and also the presence of many nonbonding states in vacancy systems, the instability caused in the 5*d* SAV hydrides is greatly reduced and is much closer to the instability caused in 3*d* and 4*d* hydrides than those in the ideal cases. Therefore, the reduction of E_v is more significant in the cases of 5*d* metals than others, as we showed in section 3.

Similar features also exist in the cases of group IB metals, i.e., the appearance of e_g-e_g bonding states at the lowest energy levels and many nonbonding states. In particular, the e_g nonbonding states appeared at ~2.0 eV (for example, in the Au case) are available to form bonding with H, as indicated in Figure 5. Note that the similar states also exist in the cases of group IIIV metals, but they are unoccupied and above the Fermi levels. In addition, from Mulliken charge analyses we see that compared to their corresponding metals, the amounts of *d* electrons in SAV hydrides of group IB metals actually decrease, meaning more *d* electrons are involved in forming bonding with H. Therefore, the vacancy formation energies are significantly reduced in SAV hydrides compared to those in pure metals.

3.4. An Alternative Pathway to form SAV Hydride from Alloy. Among the systems investigated, Palladium metal has long been regarded as an attractive H-storage medium, ever since the discovery in 1886 by Graham.[41] Moreover, the first SAV hydride discovery was made on Pd. Thus, it is worth commenting on our results of Pd hydrides. From our calculations, although the Pd SAV hydride could be stable with respect to pure Pd at an appropriate temperature, it is less stable than the ideal hydride implying that an energy barrier must be overcome if the SAV formation were to occur via the ideal hydride. On the other hand, the vacancy formation energies in noble metals and 5*d* metals are negative, indicating that their SAV hydrides could be easily formed if the ideal hydrides were obtained. Utilizing these results, here we propose a reaction pathway by alloying a noble metal and Pd, leading to an easier route for SAV formation from ideal hydrides. It is worth re-emphasizing that the relative stability between SAV and ideal hydrides (i.e., $M_4H_4 \rightarrow M_3VacH_4 + M(bulk)$) is unaffected by the H_2 chemical potential. In other words, a feasible pathway to form SAV hydrides from ideal hydrides is significant because it does not resort to extreme conditions. Here, we chose a Cu and Pd alloy to realize a reaction to generate an SAV hydride. Cu is chosen because it is relatively inexpensive and because ordered Cu−Pd alloys have been reported.[42] We have tried different compositions of Cu and Pd, and found that a $CuPd_3$ alloy may be a good candidate.

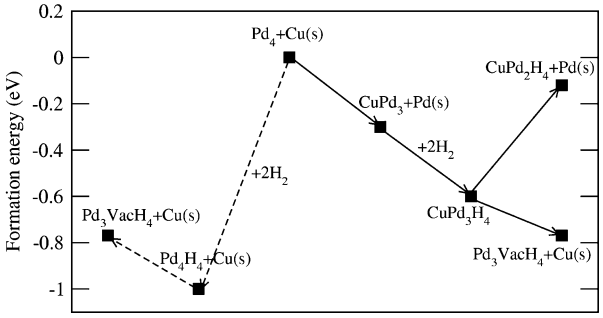

Figure 6. Calculated formation energies of Pd_3VacH_4. Two reaction paths are shown: (i) starting from pure Pd metal (the dashed lines on the left-hand side); and (ii) starting from the $CuPd_3$ alloy (the solid lines on the right-hand side).

As shown schematically in Figure 6, starting from the ideal Pd (the zero energy in the Figure) we have found that the process to generate the ordered $CuPd_3$ alloy is exothermic with a formation energy of −0.30 eV. Hydriding the alloy also has an exothermicity of 0.32 eV. There are two alternative paths to create metal vacancies from the ideal hydride, $CuPd_3H_4$. As shown in Figure 6, the formation of Pd_3VacH_4 is clearly favored with a formation energy of −0.16 eV, whereas the reaction to form $CuPd_2H_4$ is endothermic by 0.50 eV. The more favorable path to form Pd_3VacH_4 can be understood from the fact that the Cu−H bond is weaker than Pd−H bond, as can be seen from Table 2 or 3. In addition, the ideal hydride of $CuPd_3$ alloy has a heat of formation (per H) of −0.08 eV, which is significantly more positive than that of Pd_4H_4 (−0.35 eV). In fact, it is even more positive than the heat of formation of Ni_4H_4 (−0.18 eV), whose vacancy formation energy is close to zero. From our discussion in above sections: the less stable the ideal hydride, the more stable the SAV hydride, thus, the SAV hydride (Pd_3VacH_4) should be more stable than its corresponding ideal hydride, $CuPd_3H_4$. For the sake of comparison, the mechanism to form Pd_3VacH_4 directly from pure Pd is also drawn on the left-hand side of the Figure. In all the calculations, the ZPE and entropy effects are included.

4. Conclusions

In this work, we have carried out detailed investigations on the formation of SAV hydrides of a series of fcc transition metals. Some of our key findings and implications are now briefly recapped as follows.

(1) In agreement with the experimental suggestions, we have found that the vacancy formation energies in metals reduce substantially due to the insertion of H.

(2) We have shown that the conventional understanding of vacancy formation energies or the stabilities of hydrides in terms of cohesive energies is incomplete. The lattice relaxation (in the case of pure metals) and H insertion (in the cases of hydrides) need to be taken into account.

(3) Although ideal hydrides of 5*d* metals and noble metals are unstable compared to their corresponding pure metals, the SAV hydrides are found to be more stable than the corresponding ideal hydrides, whereas opposite results exist in the cases of Ni, Rh, and Pd.

(4) We have also demonstrated that the previous explanation of the SAV formation mechanism based on the configurational entropy effects is incorrect. The entropy change from ideal

(41) Graham, T. *Proc. R. Soc.* **1869**, *17*, 212.
(42) Thornton, J. M. C.; Unsworth, P.; Newell, M. A.; Weightman, P.; Jones, C.; Bilsborrow, R.; Norman, D. *Europhys. Lett.* **1994**, *26*, 259.

hydrides to SAV hydrides is not significant enough to alter their relative stabilities, although the entropy effects favor SAV formation.

(5) The electronic structure is shown to be crucial in determining the SAV formation mechanism and the relative stabilities of metal hydrides. We have found that in the two hydriding processes of M_4 and M_3Vac, more electrons are transferred from metals to H and fewer electrons are promoted to the high-energy antibonding states in the latter than in the former. Thus, M_3Vac is stabilized by the H-metal bonding in SAV hydrides to a much greater extent than M_4 is stabilized by the H-metal bonding in ideal hydrides. Consequently, the vacancy formation energy is reduced substantially.

(6) Finally, we have shown that instead of generating a Pd SAV hydride from pure metal, the former may be generated via a more kinetically favorable path from a $CuPd_3$ alloy.

Acknowledgment. Support of the EPSRC via the TCM/CUC[3] Portfolio Award is gratefully acknowledged. A.A. is also grateful to the NWO for support through Grant No. B 70-339, and Theoretical Chemistry Group of the Vrije Universiteit Amsterdam, and where part of this work was done.

JA050475W